Macromolecules

Article

pubs.acs.org/Macromolecules

Multilength Scale Studies of the Confined Crystallization in Poly(L-lactide)-*block*-Poly(ethylene glycol) Copolymer

Jingjing Yang,[†,‡] Yongri Liang,[†,*] Jun Luo,[†,‡] Chuanzhuang Zhao,[†] and Charles C. Han[†,*]

[†]Beijing National Laboratory for Molecular Sciences, Joint Laboratory of Polymer Science and Materials, Institute of Chemistry, Chinese Academy of Sciences, Beijing 100190, China

[‡]Graduate School of Chinese Academy of Sciences, Beijing 100049, China

ABSTRACT: In this work, we investigated the structure and morphology formation in crystalline−crystalline diblock copolymer of poly(L-lactide)-*block*-poly(ethylene glycol) (PLLA-*b*-PEG) on different length scales with optical microscopy (OM), atomic force microscopy (AFM), synchrotron time-resolved small-angle X-ray scattering (TR-SAXS) and wide-angle X-ray scattering (WAXS) methods. The PLLA-*b*-PEG copolymer with 5000 of number-average of molecular weight of PLLA and PEG blocks was used in this work. The structure and morphology of PLLA-*b*-PEG copolymers were formatted by a two-step crystallization process: i.e., the PLLA block crystallized fully at 110 °C in the first step, and then the PEG block crystallized fully at 30 °C in the second step. The OM, AFM, and SAXS results indicated that the PEG block crystallized in the multilength scales amorphous regions confined by PLLA crystals. The PEG block crystallized not only in the interlamellar regions of PLLA crystals, but also in the interfibrillar regions of PLLA. However, the subsequent crystallization of PEG block did not alter the foregoing spherulitic morphology of PLLA on the micrometer scale.

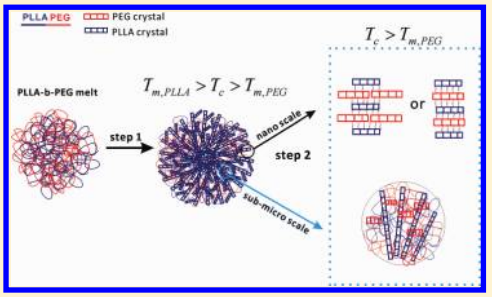

INTRODUCTION

The subject of crystallization in block copolymers has attracted much attention in the past few decades as reviewed by several researchers,[1−5] since the crystallization is an important process to control the solid state structure and morphology in crystalline block copolymers.

The crystallization behaviors of crystalline−crystalline diblock copolymer potentially offer even richer possibilities than crystalline−amorphous diblock copolymer because that the ultimate phase and crystalline morphology is determined by not only microphase separation but also crystallization of both blocks. Interplay between both blocks during crystallization process is one of the important aspects of crystallization in the crystalline−crystalline diblock copolymer. When the melting temperatures of both blocks, T_{m1} and T_{m2}, are close to each other, a simultaneous crystallization phenomenon of both blocks can be obtained and therefore a unique crystallization behavior is expected such as in the case of poly(ethylene oxide)-*block*-poly(ε-caprolactone) (PEO-*b*-PCL).[6] Conversely, when the melting temperature of one block, T_{m1}, is far above the other, T_{m2} (i.e., $T_{m1} \gg T_{m2}$), a completely different behavior can be observed. If both blocks are miscible or weakly segregated in the molten state, through quenching, the block 1 with higher melting temperature (T_{m1}) will start to crystallize first without any confinements, and the second block with lower melting temperature, T_{m2}, should crystallize under a confined condition of existing crystallized morphology. Such crystallization behaviors have already been studied in several different crystalline−crystalline diblock copolymers including poly(L-lactide)-*block*-poly(ε-caprolactone) (PLLA-*b*-PCL) copolymer,[7−9] and poly(L-lactide)-*block*-poly(ethylene oxide) (PLLA-*b*-PEO) copolymer[10−18] etc. Although the crystallization behaviors have been widely studied in the crystalline−crystalline diblock copolymers, there is still lack of knowledge about the interplay between crystallization kinetics of both blocks.

PLLA-*b*-PEG copolymer is one of the most important biodegradable crystalline−crystalline diblock copolymer with excellent properties such as biodegradability, biocompatibility, innocuity, tissue absorbability, and so on. It has great application potential in medical area such as porogen in PLLA scaffold,[19] drug delivery media[20] and tissue antiadhesion film material with anti-inflammatory drug in surgical operation[21] as well as for the fundamental studies of confined crystallization. The introduction of poly(ethylene glycol) (PEG) component as block is expected to improve the physical properties of poly(L-lactide) (PLLA), as well as enhance its degradation resistance, adjust its hydrophobicity, and hydrophilicity balance and improve its drug release properties. Up to now, several research works have already been performed for different applications and fundamental research. For example, Sun et al.[10] studied the crystallization behaviors and crystalline morphology evaluation in a series of PLLA-*b*-PEG with identical methoxy-terminated poly(ethylene glycol) molecular weights and different PLLA molecular weights using polarized optical microscopy (POM) and atomic force microscopy

Received: November 14, 2011
Revised: March 11, 2012
Published: April 30, 2012

(AFM) techniques. They observed banded spherulites morphology in all the copolymers with POM, and observed lozenge-shaped single crystal with screw dislocations via AFM. They also investigated that effect of PEG block crystallization on spherulitic morphology, and they found that the crystallization spherulitic morphology was not changed before and after the PEG block crystallization on the micrometer scale. However, they did not analyze the detailed effect of PEG crystallization on the morphology in the nanometer scale. Afterward, Yang et al.[12] studied the single crystal of PLLA and PEG blocks in PLLA-*b*-PEG thin films with transmission electron microscopy (TEM), selected-area electron diffraction (SAED) and real-time AFM methods. They observed two types of crystal morphology: lozenge shape or hexagonal shape multilayer and layer-dendritic crystal. They found that the foregoing crystallization of PLLA block had an effect on the crystal orientation of the PEG block with PEG block crystallized epitaxially on the PLLA crystal. Shin et al.[13] investigated the morphology of PLLA-*b*-PEO-*b*-PLLA triblock copolymer with POM and small-angle X-ray scattering (SAXS) methods. They observed spherulite morphology by POM during sequential crystallization of PLLA and PEO by slowly cooling (−2 °C/min) the sample from the melt. In the resultant spherulitic morphology, the retardation of polarized light was additive, and the sign of the spherulite (negative) was preserved when the PEO crystallized within the framework established by the PLLA crystals. And their results of wide-angle X-ray diffraction (WAXD) studies on shear aligned triblock copolymers indicated that the PLLA and PEO crystals adopt the same average orientation. Yang et al.[14] investigated the effect of the PLLA block length on the confined crystallization behavior, melting behavior, and nonisothermal crystallization kinetics of PEG blocks in PLLA-*b*-PEG diblock copolymers with differential scanning calorimetry (DSC). Huang et al.[15] analyzed the crystal unit-cell structures and the isothermal crystallization kinetics of PLLA-*b*-PEG diblock copolymers with WAXS and DSC methods. The existence of PEG blocks indeed influenced the crystallization kinetics of PLLA blocks. Most of the research works on the PLLA-*b*-PEG copolymer focused on the crystallization behaviors and morphology of PLLA blocks so far. However, they paid a little attention to the crystallization behavior and morphological features of the PEG block. It is necessary to study the structure and morphology of PLLA and PEG blocks in detail to further understand the interplay between crystallization behaviors of both blocks.

Therefore, in this work, we investigated the structure and morphology formation of PLLA-*b*-PEG copolymer on different length scales with POM, AFM, time-resolved SAXS and WAXS methods. Our results demonstrated that PEG blocks crystallized in the confined multiscale amorphous regions created by the precrystallization process of PLLA blocks. In this study, these special results were observed and reported for the first time.

EXPERIMENTAL SECTION

Material and Characterization. The PLLA-*b*-PEG copolymer sample was provided by Ji'nan Daigang Co, Ltd., in China. The polymerization process was as following: PLLA-*b*-PEG copolymer was synthesized by ring-opening polymerization of L-lactide using monomethoxy poly(ethylene glycol) (MePEG) (number-average molecular weight, M_n = 5000, Aldrich) as the macroinitiator and the Stannous octoate ($Sn(Oct)_2$) as catalyst under vacuum at certain polymerization condition. The molecular weight of PLLA block was controlled by the feed ratio of L-lactide and MePEG monomers. After polymerization, the PLLA-*b*-PEG copolymer was purified through dropping the PLLA-*b*-PEG chloroform solution into iced ethyl ether to precipitate. The M_n and polydispersity index of MePEG were 5000 and 1.04 respectively, determined by gel permeation chromatography (GPC) (Waters Co.) using polystyrene (PS) as standard and dimethylformamide (DMF) as eluent. The number-average and weight-average molecular weight of PLLA-*b*-PEG sample were 10090 and 12600 respectively, determined by GPC (Waters Co.) using PS as standard material and tetrahydrofuran (THF) as eluent. The polydispersity index of PLLA-*b*-PEG was 1.25. The chemical structure of PLLA-*b*-PEG sample was determined by ^{1}H NMR (Bruker AVANCE 400). If the end unites of PLLA block was disregarded, the M_n of PLLA block was 4900 calculated by peak analysis of ^{1}H NMR spectra based on the known M_n of PEG block. In this work, the PLLA-*b*-PEG copolymer was represented by $LA_{5k}EG_{5k}$. The physical parameters of $LA_{5k}EG_{5k}$ were summarized in Table 1. The homopolymers of PLLA (M_w = 100 000) and PEG (M_n = 5000) were also provided by Ji'nan Daigang Co, Ltd., in China.

Table 1. Physical Parameters of $LA_{5k}EG_{5k}$

	PLLA block		PEG block	
M_n	4900[a]		5000	
	5090[d]			
no. of repeat units	70		113	
weight fraction (wt %)	0.50		0.50	
volume fraction (in the melt) (v %)	0.48		0.52	
melting temperature (°C)[b]	140		53	
state	amorphous	crystalline	amorphous	crystalline
electron density (e/nm^3) at room temp[c]	396	410	368	406
density (g/cm^3)	1.248	1.29	1.124	1.239

[a] ^{1}H NMR result. [b] DSC (with a heating rate of 10 °C/min). [c] Calculated by $\rho_e = (Z(\text{repeat unit}))/(V(\text{repeat unit})) = Z/(M_0/(d \times N_A))$, where Z is the number of electrons of the repeat unit; V is the specific volume; M_0 is the molecular weight of the repeat unit; d is density; N_A is Avogadro's constant. [d] GPC.

Preparation of Annealed Samples. The annealed $LA_{5k}EG_{5k}$ samples were prepared by two-step crystallization process using a Linkam hot stage (LTS 350). In the first step, the $LA_{5k}EG_{5k}$ samples were preheated at 180 °C for 5 min to eliminate thermal history and then rapidly quenched to 110 °C (between melting temperatures of PLLA, $T_{m,PLLA}$, and PEG, $T_{m,PEG}$, i.e., $T_{m,PLLA}$ > 110 °C > $T_{m,PEG}$) to isothermally crystallize PLLA block for 6 h. In the second step, $LA_{5k}EG_{5k}$ samples were isothermally crystallized at 30 °C (below $T_{m,PEG}$) for 2 h.

Optical Microscopy. The POM and phase contrast microscopy (PCM) images of $LA_{5k}EG_{5k}$ were observed by an optical microscope (Olympus BX51) equipped with an Olympus camera (C-5050ZOOM). A first-order red plate (λ = 530 nm) was used as compensator. The sample temperature was controlled by a Linkam (LTS 350) hot stage. The $LA_{5k}EG_{5k}$ samples for optical microscope observation were prepared about 20 μm of thickness on a clean glass slide and covered with a cover glass.

Atomic Force Microscopy. AFM images of the annealed $LA_{5k}EG_{5k}$ samples were recorded by a commercial scanning probe Nanoscope multimode IIIA (Vecco) operating in tapping mode. A high-temperature heater accessory was used to control the sample temperature during AFM analysis. A silicon cantilever tip was used for measurements of AFM images. The resonance frequency was 300 kHz and the scan rate was 20 μm/s. The scanning density was 512 lines per frame.

Synchrotron Time-Resolved Small- and Wide-Angle X-ray Scattering. Synchrotron time-resolved small and wide-angle X-ray scattering (TR-SAXS and TR-WAXS) measurements were performed

at BL16B1 and BL14B1 beamline in Shanghai Synchrotron Radiation Facility (SSRF), China, respectively. Two-dimensional (2D) Mar165 and Mar345 detectors were used to collect the2D SAXS and WAXS patterns, respectively. The wavelength of the incident X-ray was 1.24 Å for both SAXS and WAXS, and the sample to detector distance (SDD) was 2820 mm for SAXS and 224.5 mm for WAXS measurements. Silver behenate ($AgC_{22}H_{43}O_2$) and Silicon powder were used as standard materials for calibration of the scattering vector of SAXS and WAXS, respectively. The air and parasitic scattering were subtracted from original SAXS and WAXS data, respectively. An INSTEC (STC200) hot stage was used to control sample temperatures, which was calibrated by temperature calibrator (Fluker 724) with K type of very fine thermocouple (Omega) before use.

SAXS Analysis. The normalized 1D correlation function ($\gamma_1(r)$) is defined as[22,23]

$$\gamma_1(r) = \int_0^\infty I(q)q^2\cos(qr)\,dq/Q \quad (1)$$

where $I(q)$ is the scattering intensity, q is the scattering vector defined as $q = (4\pi \sin\theta)/\lambda$ (2θ is the scattering angle), and r is the direction along the lamellar stack.

The scattering invariant, Q, is defined as

$$Q = \int_0^\infty I(q)q^2\,dq \quad (2)$$

Because of the finite q range of experimental SAXS data, extrapolation of the 1D SAXS data to both the low and high q ranges are necessary for the integration of the intensity, $I(q)$. Extrapolation to low q was performed using an intensity profiles based on Guinier's law,[24] and the extension of the intensity to large q values can be accomplished by using Porod–Ruland model.[25] The parasitic scattering and thermal fluctuation were corrected before analysis of normalized 1D correlation function.

Crystallinity. The total crystallinity ($X_{w,t}$) of the $LA_{5k}EG_{5k}$ (including both crystallinities of PLLA and PEG blocks) and the crystallinity of the PLLA block ($X_{w,PLLA}$) in the $LA_{5k}EG_{5k}$ sample were calculated based on the one-dimensional (1D) WAXS profiles of annealed $LA_{5k}EG_{5k}$ sample obtained at room temperature and 70 °C. The crystallinity was estimated by $X_w = (A_{cry})/(A_{cry} + A_{amor.})$, where, X_w is the mass crystallinity;A_{cry} and $A_{amor.}$ are the peak areas of diffraction peaks contributed by crystalline and amorphous phases in the sample, respectively. The crystallinity of the PEG blocks in the annealed $LA_{5k}EG_{5k}$ sample ($X_{w,PEG}$) was calculated by $X_{w,PEG} = X_{w,t} - X_{w,PLLA}$. The crystallinities of $X_{w,t}$ and $X_{w,PEG}$ were obtained by peak fitting analysis. The crystallinities of PLLA and PEG blocks in the annealed $LA_{5k}EG_{5k}$ sample were obtained by peak fitting analysis as 0.23 and 0.33, respectively

RESULTS AND DISCUSSIONS

Time-Resolved WAXS. In order to clarify the structure formation of $LA_{5k}EG_{5k}$ sample during the two-step crystallization process, TR-WAXS measurement was performed. Figure 1 showed the 1D WAXS profiles of $LA_{5k}EG_{5k}$ sample obtained at 110 and 30 °C for different crystallization time. At 110 °C, only the PLLA component is crystallizable and the PEG component still keeps a molten state. At the beginning of the isothermal crystallization at 110 °C, the WAXS profile showed a broad Gaussian peak. It indicates that the sample reserved an amorphous state at the beginning. The crystallization of PLLA in $LA_{5k}EG_{5k}$ sample started at around 10 min and almost completed at about 60 min as shown in Figure 1 and 2. In the subsequent crystallization at 30 °C, we observed an obvious diffraction peak appeared at 2θ = 18.7°, which corresponds to (032)/($\bar{1}$24)/(112) crystal planes of PEG crystals. The crystal structure of PEG crystal is monoclinic with crystal unit cell parameters of a = 0.805 nm, b = 1.304 nm, c = 1.984 nm, and β = 125.4° and a 7_2 helical chain

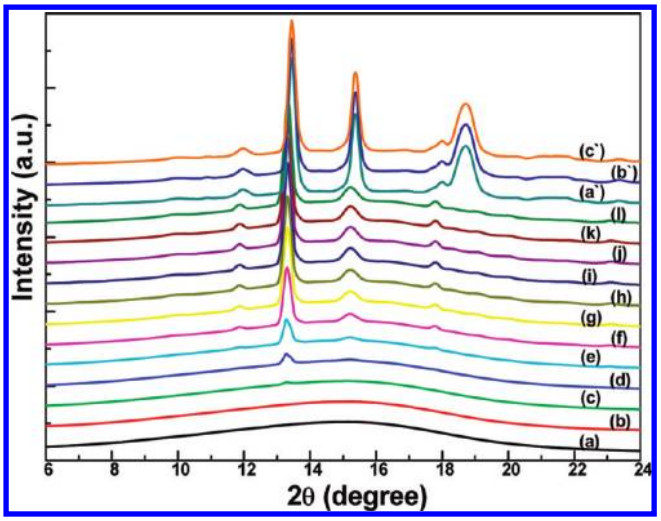

Figure 1. Time-resolved WAXS profiles of $LA_{5k}EG_{5k}$ sample obtained during isothermal crystallization processes at 110 (a–l) and 30 °C (a′–c′), respectively: (a) 0 min; (b) 5 min; (c) 10 min; (d) 15 min; (e) 19 min; (f) 28 min; (g) 35 min; (h) 40 min; (i) 45 min; (j) 50 min; (k) 60 min; (l) 120 min; (a′) 3 min; (b′) 10 min; (c′) 30 min.

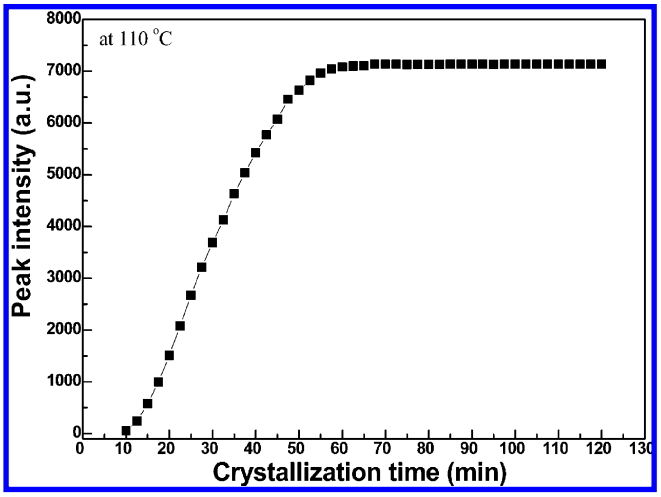

Figure 2. Intensities of peak at 13.28° in $LA_{5k}EG_{5k}$ sample obtained during isothermal crystallization at 110 °C.

conformation.[26] In addition, the peaks at 13.28° and 15.2° were obviously shifted to 13.44° and 15.38°, respectively, after crystallization at 30 °C.

It is well-known that the PLLA has three different kinds of crystal modifications, α-form,[27] β-form[28,29] and γ-form[30] crystal modifications. The most common and stable polymorph, α-form crystal, has a 10_3 helical chain conformation, and has two chains in an orthorhombic unit cell with parameters of a = 1.06 nm, b = 0.61 nm, and c = 2.88 nm.[27] This form can be developed from the melt or solution under normal conditions in PLLA homopolymer. A new crystalline form, the a′-form, has also been reported.[31] The a′-form is reported to be a "disordered crystal" having the same 10_3 conformation as in α-form but has a pseudohexagonal unit cell with a = b=0.62 nm, c = 2.88 nm, The a′-form usually forms at lower crystallization temperatures and could transform to the stable α-form phase during the heating process.[32] In the α-form many X-ray diffractions appear, including: (010), (110/200), (203), (204), (015), and (207) planes which correspond to the Bragg

dx.doi.org/10.1021/ma202505f | Macromolecules 2012, 45, 4254–4261

angles 2θ (X-ray wavelength at 0.154 nm) of 15°, 16.7°, 19.1°, 21°, 22.3°, and 27.4°, respectively. However, in the a′-form, reflection peaks appear at 16.4°, 18.7° and 24.5° (X-ray wavelength at 0.154 nm). Thus, in our case, the peaks at 13.28° and 15.2° should be contributed by PLLA a′-form crystals, and the peaks at 13.44° and 15.38° should be contributed by PLLA α-form crystals. We also confirmed that the infrared peaks of PLLA α-form crystals were significantly enhanced after crystallization at 30 °C (data not shown). Therefore, we considered that a transformation of PLLA crystals from a′-form to α-form was happening when the PEG crystallized at 30 °C. It is quite different from the PLLA homopolymer. One of the possibilities is that the PLLA crystals may be stretched or sheared by the tethered PEG blocks during the PEG block crystallization process. Recently, Chen et al.[33] reported that the a′-form phase of PLA films does not transform to α- or β-crystals on uniaxial drawing as varying the value of DR. The mechanism of phase transformation in PLLA-*b*-PEG copolymer is not clear at present. We will discuss this issue further.

Structure Formation of $LA_{5k}EG_{5k}$ Copolymer on Nanometer Scale. In order to investigate the structure formation on the nanometer scale, we observed time-resolved 2D SAXS patterns of $LA_{5k}EG_{5k}$ sample during isothermal crystallization processes. Figure 3 showed the time-resolved

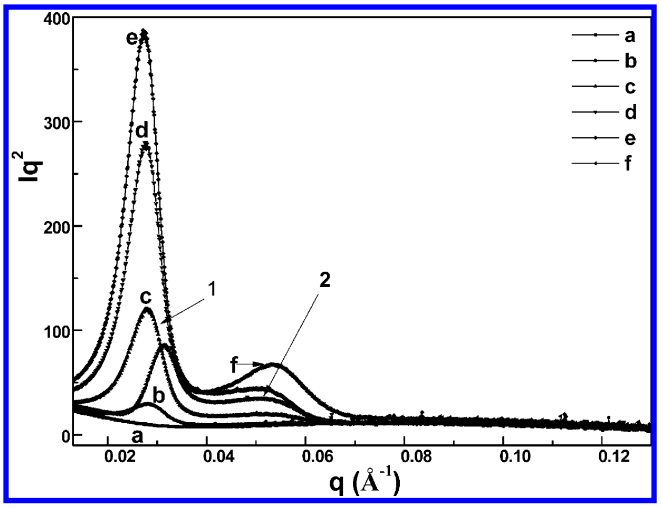

Figure 3. Lorentz-corrected 1D SAXS profiles of $LA_{5k}EG_{5k}$ copolymer obtained at selected crystallization time during isothermal crystallization process at 110 °C (a–e) and then at 30 °C (f): (a) 110 °C for 0 min; (b) 110 °C for 12 min; (c) 110 °C for 25 min; (d) 110 °C for 40 min; (e) 110 °C for 90 min; (f) 30 °C for 10 min.

Lorentz-corrected 1D SAXS profiles of the $LA_{5k}EG_{5k}$ sample obtained at selected crystallization time during both isothermal crystallization processes at 110 and 30 °C. At the beginning of the crystallization at 110 °C, no scattering peak was observed in the SAXS profile. The electron density of amorphous PLLA (397 e/nm^3) is significantly different from that of amorphous PEG (345 e/nm^3) at 110 °C. Thus, absence of the scattering peak indicated that the microphase separation of PLLA and PEG blocks was absence in the molten state. When the $LA_{5k}EG_{5k}$ sample crystallized at 110 °C for 12 min, a scattering peak (peak 1) was clearly observed at 0.0282 Å^{-1} and the intensity of peak 1 increased with crystallization time increasing due to the crystallization of PLLA (Figure 1). On the other hand, a weak and broad peak at 0.0517 Å^{-1} (peak 2) appeared in the SAXS profile obtained at about 18 min as shown in Figure 3 or Figure 4. The ratio of peak position of peak 2 and peak 1 (q_2/q_1) was 1.83. It indicates that the peak 2 is not high

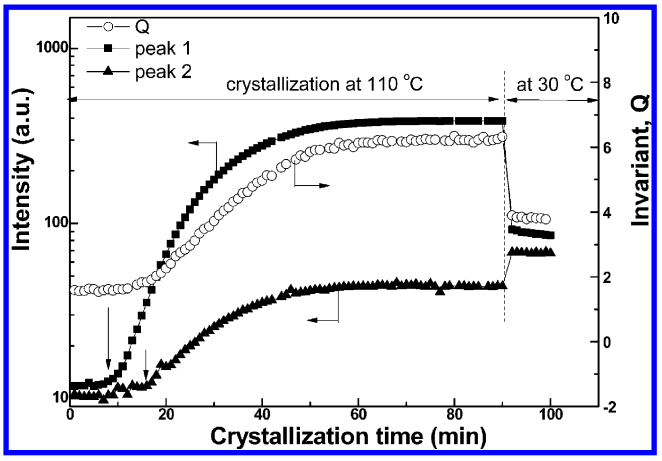

Figure 4. Intensities of peak 1 and 2 from SAXS profiles, and invariant of $LA_{5k}EG_{5k}$ sample obtained at different crystallization time during isothermal crystallization processes at 110 °C and then at 30 °C.

ordering peak from lamellar structure. The intensities of peak 1 and 2, and invariant, Q, increased with crystallization time increasing and reached to maximum values at around 60 min at 110 °C. It means that the peak 2 appeared accompanying with the crystallization process of PLLA block. In the crystallization process of PLLA block, the amorphous PEG block should be rejected from the front of PLLA crystals, resulting in the local concentration of PEG block increasing. Furthermore, the rejected PEG blocks should be trapped within interlamellar spaces due to tethered with PLLA blocks. Therefore, the peak 1 should be contributed by PLLA lamella, whereas, the peak 2 should be contributed by crystallization induced segregation structure.

The long period of PLLA lamellar structure (L_1) was 22.1 nm at the beginning, however, the L_1 increased with crystallization time increasing after peak 2 appeared (about 20 min) as shown in Figure 5. The L_1 increased from 22.1 to 23.1 nm, finally. The long period was obtained by $L_1 = 2\pi/q_1$,

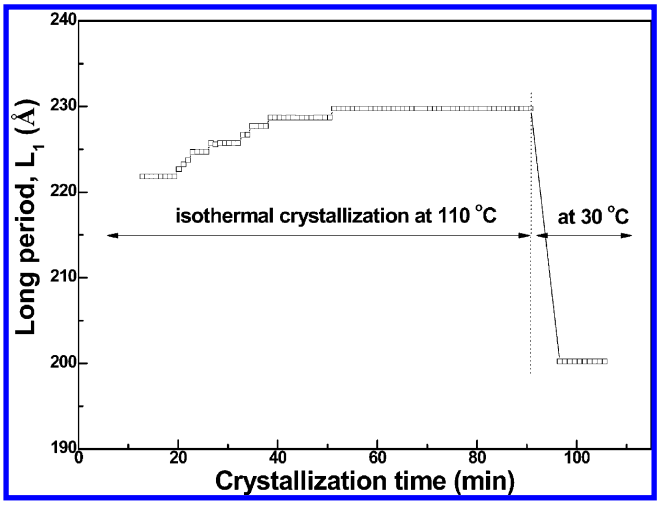

Figure 5. Long period (L_1) of $LA_{5k}EG_{5k}$ obtained at different crystallization time during isothermal crystallization process at 110 °C and then at 30 °C.

dx.doi.org/10.1021/ma202505f | *Macromolecules* 2012, 45, 4254–4261

where q_1 is the scattering vector at peak 1. The possibilities of the long period of PLLA block increasing during crystallization includes two aspects: one was that the tethered amorphous PLLA segments may be stretched by crystallized PLLA segments, and the other was that the volume of the amorphous PEG block segregated by the PLLA crystallization was larger than the volume of PLLA, because the density of PEG was lower than PLLA.

When the $LA_{5k}EG_{5k}$ sample crystallized at 30 °C, subsequently, the invariant and intensity of peak 1 suddenly dropped, whereas the intensity of peak 2 (the position of peak 2 shift to higher q) significantly increased as shown in Figure 3 and 4. Meanwhile, the intensity of peak 1 decreased about 78%, and the intensity of peak 2 increased about 125%. The invariant, Q, also decreased about 38.5%. In the semicrystalline homopolymer, it is well-known that the invariant is proportional to the electron density difference between the two phases (crystalline and amorphous phase) and the volume fractions of the two phases based on two phase model. The electron densities of amorphous and crystalline phases of PEG are 345 and 406 e/nm^3, respectively. And the electron density of crystalline phase of PLLA is 410 e/nm^3. Therefore, the invariant or intensity of peak 1 decreasing was contributed from decreasing the electron density difference in the PLLA lamellae. It can be explained that the PEG crystals inserted in the regions of interlamella of PLLA, partially or fully (i.e., partial or full insertion model).

On the other hand, the L_1 decreased about 13.4% (from 23.1 to 20.0 nm) by subsequent crystallization at 30 °C. The density of amorphous PEG was calculated as 1.053 and 1.124 g/cm^3 at 110 and 30 °C respectively.[34] And, the density of crystalline phase of PEG is 1.239 g/cm^3. If we only considered the thermal shrinking of PEG, the volume change was calculated only 6%. Whereas, if we assumed the amorphous phase of PEG entirely converted to crystalline phase, the volume change was calculated as 14.7%. Thus, the L_1 change is also supporting the partial or full insertion model.

The 1D correlation function can provide the structure parameters of lamella. Since the PLLA and PEG blocks were forming individual lamellar structures, we considered the 1D correlation function of annealed $LA_{5k}EG_{5k}$ is a superposition of two periodic structures from the individual PLLA and PEG lamella. Figure 6 showed the normalized 1D correlation function of $LA_{5k}EG_{5k}$ sample isothermally crystallized at 110 °C for 90 min and subsequently crystallized at 30 °C. The normalized 1D correlation function of $LA_{5k}EG_{5k}$ sample only showed one periodic peak when the PLLA crystallized alone (Figure 6a), whereas showed two different periodic peaks when the PEG crystallized subsequently at 30 °C (Figure 6b). The crystalline layer thickness of PLLA was estimated by the normalized 1D correlation function of $LA_{5k}EG_{5k}$ obtained at 110 °C. On the basis of the crystallinity (X_w = 0.23) of PLLA in $LA_{5k}EG_{5k}$, we assigned the smaller layer thickness (l_1) to crystalline thickness. The long period (L_{PLLA}) and crystalline thickness of PLLA ($l_{c,PLLA}$) was determined as 23.5 and 6.1 nm in the Figure 6a. It was in good agreement with the long period obtained by Bragg's law from the SAXS profiles of $LA_{5k}EG_{5k}$ at 110 °C (23.1 nm). The linear crystallinity of PLLA ($X_{l,PLLA}$ = $l_{c,PLLA}/L_{PLLA}$) was calculated as 0.26 (for the $LA_{5k}EG_{5k}$ copolymer). In order to calculate the amorphous thickness of PLLA in crystallized PLLA lamellae, we assumed that the amorphous chains of PLLA were fully stretched. If the end group is neglected, the maximum length of the molecules in the fully extended form is $L = L_m \times N$, where L_m is the length of the repeat unit along the chain axis in the helical state and N is the degree of polymerization. Thus, the fully extended chain length of PLLA, $L_{0,PLLA}$, can be calculated by $L_{0,PLLA}$ = (2.88/10) × (5000/72) ≅ 20 nm. And, the possible number of chain folding in PLLA crystals can be estimated by $n_{f,PLLA} = (L_{0,PLLA}/L_{c,PLLA}) - 1$, as $n_{f,PLLA}$ = 20/6.1−1 ≈ 2. Thus, the thickness of PLLA amorphous layer is (20−6.1 × (2 + 1))/2 ≈ 1 nm.

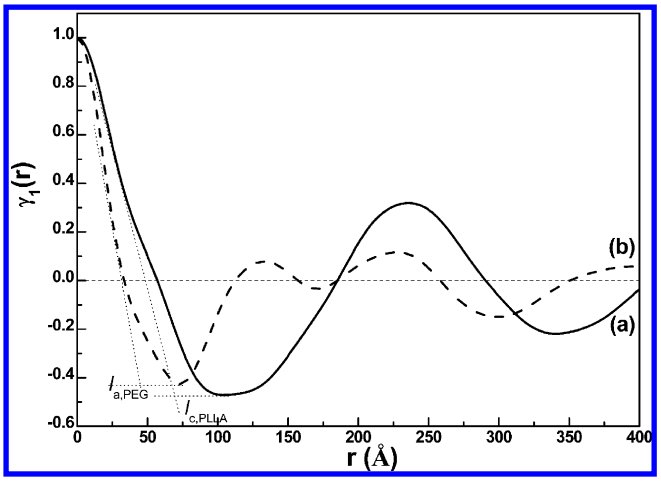

Figure 6. Normalized 1D correlation function of $LA_{5k}EG_{5k}$ copolymer sample isothermally crystallized at 110 °C for 90 min (a) (solid line) and subsequently crystallized at 30 °C (b) (dash line).

The structure parameters of PEG were estimated from the normalized 1D correlation function of the $LA_{5k}EG_{5k}$ sample at 30 °C (Figure 6b). Figure 6b exhibited both periodic structures of PLLA and PEG lamellas. In Figure 6b, by comparison with structure parameters of PLLA block, we assigned the first minimum value (3.3 nm) for the amorphous layer thickness of PEG and the first maximum value (12.4 nm) for the long period of PEG lamellar, because the crystallinity of PEG was 0.66 in the $LA_{5k}EG_{5k}$ (by WAXS). Thus, the crystal thickness of PEG was calculated by 12.4 − 3.3 = 9.1 nm. The linear crystallinities ($X_l = l_c/l$) of PEG in lamellar stack by SAXS were calculated as 0.39 (for the $LA_{5k}EG_{5k}$ copolymer) and 0.73 (for the PEG block), respectively. The linear crystallinity of PEG in the $LA_{5k}EG_{5k}$ copolymer is in good agreement with the crystallinity of PEG estimated by WAXS. The detailed structure parameters and crystallinities of PLLA and PEG blocks in $LA_{5k}EG_{5k}$ were summarized in the Table 2.

Morphology Formation of PLLA-*b*-PEG Copolymer on Micrometer and Submicrometer Length Scales. The

Table 2. Structure Parameters and Crystallinities of PLLA and PEG in $LA_{5k}EG_{5k}$

	PLLA block	PEG block
scattering vector at maximum intensity, q_{max} (Å^{-1})	0.272	0.537
long period, L_B (nm) (Bragg's law)	23.1	11.7
long period, L (nm) (1D correlation function)	23.5	12.4
crystalline thickness, l_c (nm)	6.1	9.1
amorphous thickness, l_a (nm)	1.0	3.3
mass crystallinity, X_w (%) (WAXS) for copolymer	0.23	0.33
X_w for block	0.46	0.66
linear crystallinity (volume), (SAXS) ($X_l = l_c/L$) for copolymer	0.26	0.39
X_l for block	0.52	0.73

dx.doi.org/10.1021/ma202505f | Macromolecules 2012, 45, 4254−4261

morphology formation of PLLA-*b*-PEG copolymer on micrometer length scale was characterized by POM and PCM. The $LA_{5k}EG_{5k}$ sample showed a dendritic morphology when the sample isothermally crystallized at 110 °C for 2 h as shown in Figure 7, parts a_1, a_1', or b_1. When the $LA_{5k}EG_{5k}$ sample started

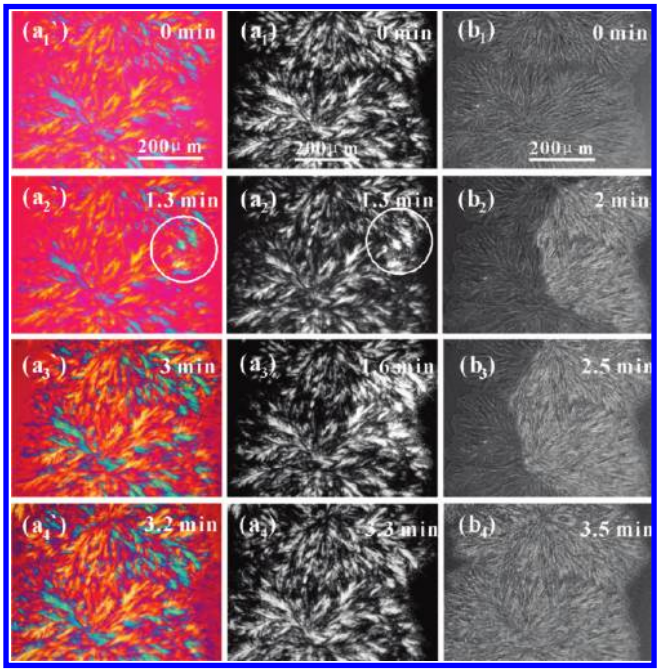

Figure 7. POM images (a′) with and (a) without compensator, and (b) PCM images of $LA_{5k}EG_{5k}$ obtained at 30 °C for different times: (a_1 $a_1'$and b_1) 0 min; (a_2) and (a_2') 1.3 min; (a_3) 1.6 min, (b_2) 2 min, (b_3) 2.5 min, (a_3') 3 min, (a_4') 3.2 min, (a_4) 3.3 min, and (b_4) 3.5 min. The first-order red plate (λ = 530 nm) was used as compensator.

to crystallize at 30 °C, a brighter area appeared at the boundary of the PLLA spherulite (marked by the circle in Figure 7, parts a_2 and a_2'), and then the brighter area rapidly propagated in all directions and covered the whole PLLA spherulite as shown in Figure 7, parts a_2−a_4, a_2'−a_4', or b_2−b_4. Furthermore, we clearly observed a lot of grain like crystals filling into the gaps in PLLA spherulites during the crystallization process. Nevertheless, those grain like crystals completely disappeared when the sample was heated to 70 °C (above the melting temperature of PEG) as shown in Figure 8. Therefore, we demonstrated that

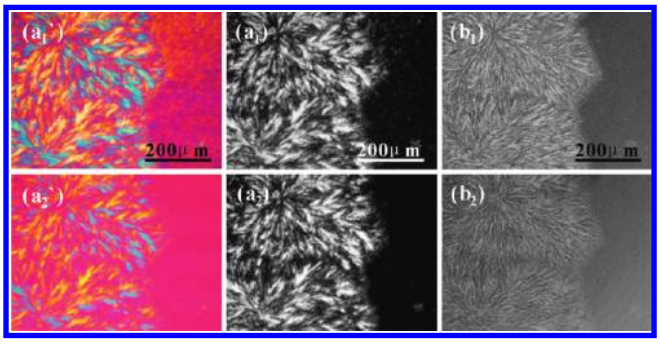

Figure 8. POM images (a′) with and (a) without compensator, and (b) PCM images of the final morphology of $LA_{5k}EG_{5k}$ sample (1) at room temperature and (2) at 70 °C. The $LA_{5k}EG_{5k}$ sample was isothermally crystallized at 110 °C for 120 min and then at 30 °C for 60 min. A first-order red plate (λ = 530 nm) was used as compensator.

the grain like crystals were PEG crystals and the PEG crystals filled in the amorphous spaces inside the PLLA spherulites. Even though the grain like crystals filled in the PLLA spherulite through the crystallization of PEG block, morphological feature of the PLLA spherulite did not change at all on the micrometer scale and the crystallization of PEG blocks just enhanced the contrast of PLLA spherulite significantly. Similar interfilling crystallization behaviors have been widely reported in the case of crystalline/crystalline blend systems.[35] In the case of crystalline/crystalline polymer blends with different melting point systems, the amorphous components (second component with lower crystallization temperature) can be rejected from the front of crystal growth into interlamellar, interfibrillar or interspherulites regions. In general, the rejection and segregation processes in crystalline/crystalline blends are dependent on miscibility, crystallization temperature of crystalline component and diffusion coefficient of amorphous component etc. In the crystalline/crystalline polymer blends, the interpenetrated crystallization phenonmenon[36] or the interfilling crystallization phenomenon[35] have been reported. However, interfilling crystallization behavior has been seldom reported in the crystalline−crystalline diblock copolymer systems. In the case of crystalline−crystalline diblock copolymer, the rejection/segregation processes of the amorphous component in the interfibrillar regions are different from that in blend systems, because the amorphous blocks (second component with lower crystallization temperature) anchored to crystalline blocks by chemical bonds. Therefore, the amorphous PEG blocks were unlikely segregated far from PLLA lamella in the case of PLLA-*b*-PEG. Accordingly, the concentration of both PLLA and PEG blocks in the PLLA interfibrillar regions should be almost similar. The crystallization induced by segregations may only exist locally in crystalline−crystalline diblock copolymers. Recently, He et al.[6] have reported unique concentric spherulitic morphologies in PCL-*b*-PEG copolymer ($M_{n,PCL}$ = 5090, $M_{n,PEG}$ = 5000). In the case of PCL-*b*-PEG, the PCL spherulites formed first, and the initial nucleation of the PEG crystals happened within a PCL spherulite at a certain time later during the isothermal crystallization. The PEG crystals grew quickly within the interlamellar regions of the PCL spherulite and then triggered the concentric growth of the outer PEG spherulite from the front of the PCL spherulite. They found that the PCL weight fractions distributed to the inner and outer portions of the concentric spherulites were equal. In this case, the crystallization temperatures of PCL and PEG were very close and the growth rate of the PEG crystal was much quicker than that of PCL crystal, even though the PEG crystal nucleated later.

In contrast with the case of PCL-*b*-PEG, the crystallization of PEG should be completely restricted by foregoing crystalline morphology of PLLA in the case of PLLA-*b*-PEG copolymer. The PEG crystals might nucleate by heterogeneity (dust or catalyst) at the boundary or inside the PLLA spherulite and then rapidly filled in the amorphous regions of PLLA spherulite and covered the whole space including interlamellar and interfibrillar regions.

However, detailed crystalline morphology of $LA_{5k}EG_{5k}$ crystals could not be observed by the OM technique due to resolution limitation. We observed the surface morphologies of annealed $LA_{5k}EG_{5k}$ sample using AFM with tapping mode at room temperature (RT). Both the flat-shaped and edge-shaped lamellar morphologies were observed in the annealed $LA_{5k}EG_{5k}$ sample as shown in Figure 9, parts b and c. We noticed that the

dx.doi.org/10.1021/ma202505f | *Macromolecules* 2012, 45, 4254−4261

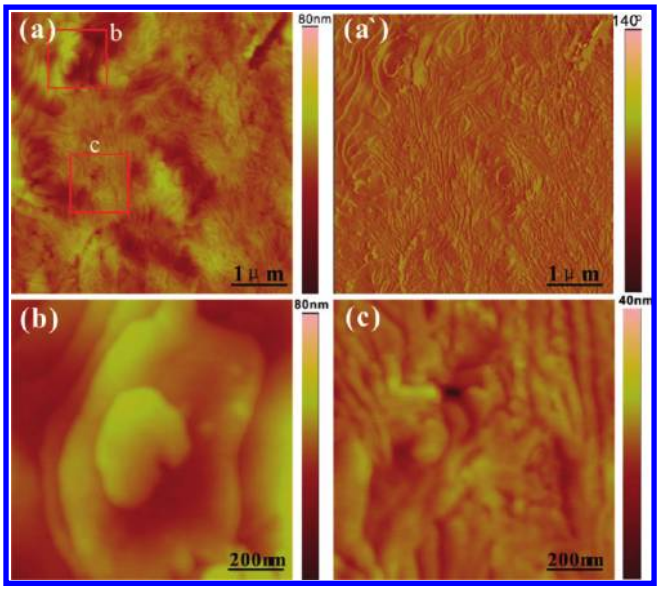

Figure 9. AFM (a) height image and (a′) phase images of annealed $LA_{5k}EG_{5k}$ sample. (b and c) Magnified height images of square boxes b and c in part a. The $LA_{5k}EG_{5k}$ sample was annealed at 110 °C for 6 h and then at 30 °C for 2 h.

flat-shaped crystals were almost located at the gaps or at the boundary of edge-shaped lamellar crystals. The sizes of flat-shaped lamellar crystals were about tens of nanometer to few hundred nanometers. Furthermore, the flat-shaped crystals packed as multilayer stacks. In order to distinguish the surface morphology features of PLLA and PEG crystals, we heated the annealed $LA_{5k}EG_{5k}$ sample to 70 °C for melting the PEG crystals. The AFM images of annealed $LA_{5k}EG_{5k}$ sample observed at RT and 70 °C were showed in Figure 10, parts a and b. We clearly observed that the flat-shaped lamellar crystals disappeared and the edge-shaped lamellar crystals were more clearly revealed after heating (marked by circles in Figure 10b). These results indicate that the flat-shaped lamellar crystals were PEG crystals and the edge-shaped lamellar crystals were PLLA crystals in the AMF images (Figure 9 and Figure 10).

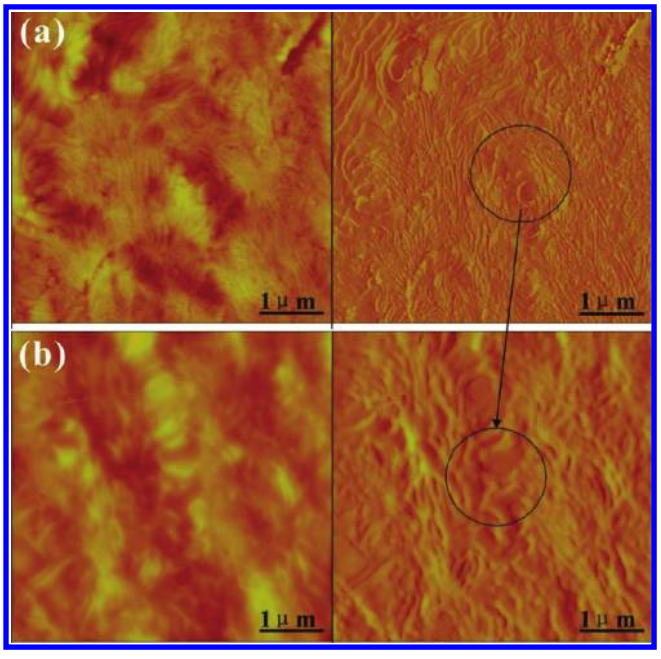

Figure 10. AFM images of annealed $LA_{5k}EG_{5k}$ sample: (a) at RT and (b) at 70 °C. The left side is AFM height images and the right side is AFM phase images.

Mechanism of Structure and Morphology Formation. The structure and morphology formation of $LA_{5k}EG_{5k}$ copolymer during two-step crystallization process was investigated with POM, PCM, AFM, WAXS, and SAXS methods. The PLLA block crystallized at 110 °C (above melting temperature of PEG), and then the PEG block crystallized at 30 °C. The SAXS results showed that the PLLA and PEG blocks were miscible in the molten state, and the PLLA block crystallized to form lamellar structure on the nanometer scale at 110 °C. Subsequently, PEG crystallized inside of the PLLA spherulites at 30 °C, however, the spherulite morphology of PLLA was not altered by the crystallization of PEG block. Meanwhile, the PEG crystallized not only in the interlamellar regions but also in the interfibillar regions of PLLA. In other words, the crystallization of PEG block took place in the nano and meso length scales of amorphous regions confined by PLLA crystals. According to multilength scales characterization of the structure formation of the PLLA-*b*-PEG copolymer, we suggested a model for the mechanism of the multilength confined crystallization behaviors of PEG block in the PLLA-*b*-PEG copolymer as schematically illustrated in Figure 11.

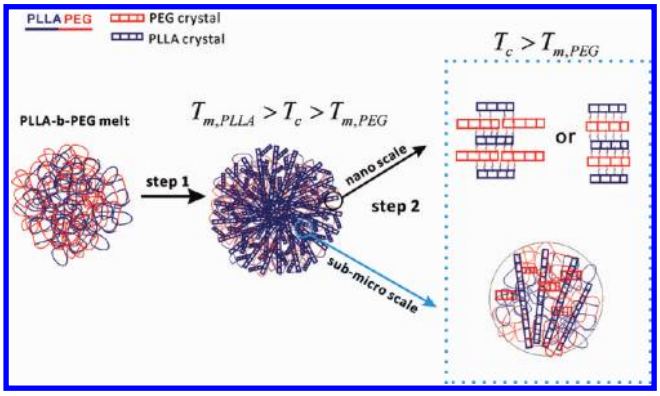

Figure 11. Schematic illustration model for mechanism of multilength scales confined crystallization of PEG block in the PLLA-*b*-PEG copolymer.

■ CONCLUSIONS

In this work, we investigated the structure and morphology formation of crystalline−crystalline diblock copolymer of PLLA-*b*-PEG copolymer on different length scales with OM, AFM, WAXS, and SAXS methods. Based on OM, AFM, and SAXS results, we found that PEG blocks crystallized at somewhere inside of the PLLA spherulites, meanwhile, the PEG crystals grew into the interlamellar and interfibillar regions of PLLA. The PEG blocks crystallized in the multilength scales spaces created by PLLA crystallization in the PLLA-*b*-PEG copolymer. Our results can provide some new insights into the mechanism of the structure and morphology formation of the melt-miscible crystalline−crystalline diblock copolymers on various length scales and help to understand the interplay between crystallization behaviors of both crystallizable blocks in the crystalline−crystalline diblock copolymers.

dx.doi.org/10.1021/ma202505f | *Macromolecules* 2012, 45, 4254−4261

AUTHOR INFORMATION

Corresponding Author

*(Y.L.) E-mail: liangyr@iccas.ac.cn). (C.C.H.) E-mail: c.c.han@iccas.ac.cn. Telephone: +86 10 82618089. Fax: +86 10 62521519.

Notes

The authors declare no competing financial interest.

ACKNOWLEDGMENTS

This research work was supported by National Natural Science Foundation of China (Young scientist fund, No. 21004070) and partially supported by the project sponsored by the Scientific Research Foundation for the Returned Overseas Chinese Scholars, State Education Ministry. The synchrotron SAXS experiments were supported by Shanghai Synchrotron Radiation Facility in China (10sr0149 and 10sr0582).

REFERENCES

(1) Hamley, I. W. *Adv. Polym. Sci.* **1999**, *148*, 113−137.
(2) Hamley, I. W., *Developments in block copolymer science and technology*. Wiley Online Library: Chichester, U.K., 2004.
(3) Müller, A. J.; Arnal, M. L.; Balsamo, V. In *Lecture Notes in Physics: Progress in Understanding of Polymer Crystallization*; Springer: Berlin, 2007; Vol. *714*, pp 229−259.
(4) Müller, A. J.; Balsamo, V.; Arnal, M. L. *Adv. Polym. Sci.* **2005**, *190*, 1−63.
(5) Castillo, R. V.; Müller, A. J. *Prog. Polym. Sci.* **2009**, *34*, 516−560.
(6) He, C.; Sun, J.; Zhao, T.; Hong, Z.; Zhuang, X.; Chen, X.; Jing, X. *Biomacromolecules* **2006**, *7*, 252−258.
(7) Kim, J. K.; Park, D. J.; Lee, M. S.; Ihn, K. J. *Polymer* **2001**, *42*, 7429−7441.
(8) Hamley, I. W.; Castelletto, V.; Castillo, R. V.; Müller, A. J.; Martin, C. M.; Pollet, E.; Dubois, P. *Macromolecules* **2005**, *38*, 463−472.
(9) Castillo, R. V.; Müller, A. J.; Raquez, J. M.; Dubois, P. *Macromolecules* **2010**, *43*, 4149−4160.
(10) Sun, J.; Hong, Z.; Yang, L.; Tang, Z.; Chen, X.; Jing, X. *Polymer* **2004**, *45*, 5969−5977.
(11) Zhang, J.; Duan, Y.; Domb, A. J.; Ozaki, Y. *Macromolecules* **2010**, *43*, 4240−4246.
(12) Yang, J.; Zhao, T.; Zhou, Y.; Liu, L.; Li, G.; Zhou, E.; Chen, X. *Macromolecules* **2007**, *40*, 2791−2797.
(13) Shin, D.; Shin, K.; Aamer, K. A.; Tew, G. N.; Russell, T. P.; Lee, J. H.; Jho, J. Y. *Macromolecules* **2005**, *38*, 104−109.
(14) Yang, J.; Zhao, T.; Cui, J.; Liu, L.; Zhou, Y.; Li, G.; Zhou, E.; Chen, X. *J. Polym. Sci., Part B: Polym. Phys.* **2006**, *44*, 3215−3226.
(15) Huang, C.; Tsai, S.; Chen, C. *J. Polym. Sci., Part B: Polym. Phys.* **2006**, *44*, 2438−2448.
(16) Huang, S.; Jiang, S.; An, L.; Chen, X. *J. Polym. Sci., Part B: Polym. Phys.* **2008**, *46*, 1400−1411.
(17) Kim, K.; Chung, S.; Chin, I.; Kim, M.; Yoon, J. *J. Appl. Polym. Sci.* **1999**, *72*, 341−348.
(18) Lee, S. Y.; Chin, I. J.; Jung, J. S. *Eur. Polym. J.* **1999**, *35*, 2147−2153.
(19) Kim, H. D.; Bae, E. H.; Kwon, I. C.; Pal, R. R.; Nam, J. D.; Lee, D. S. *Biomaterials* **2004**, *25*, 2319−2329.
(20) He, C.; Kim, S. W.; Lee, D. S. *J. Controlled Release* **2008**, *127*, 189−207.
(21) Lee, J. H.; Go, A. K.; Oh, S. H.; Lee, K. E.; Yuk, S. H. *Biomaterials* **2005**, *26*, 671−678.
(22) Strobl, G. R.; Schneider, M. J. *J. Polym. Sci., Part B: Polym. Phys.* **1980**, *18*, 1343−1359.
(23) Roe, R., *Methods of X-ray and neutron scattering in polymer science*; Oxford University Press: New York: 2000, P201.
(24) Guinier, A.; Fournet, G.; Walker, C. B.; Vineyard, G. H. *Phys. Today* **1956**, *9*, 38.
(25) Ruland, W. J. *J. Appl. Crystallogr.* **1971**, *4*, 70−73.
(26) Zhu, L.; Cheng, S. Z. D.; Calhoun, B. H.; Ge, Q.; Quirk, R. P.; Thomas, E. L.; Hsiao, B. S.; Yeh, F.; Lotz, B. *J. Am. Chem. Soc.* **2000**, *122*, 5957−5967.
(27) Kobayashi, J.; Asahi, T.; Ichiki, M.; Oikawa, A.; Suzuki, H.; Watanabe, T.; Fukada, E.; Shikinami, Y. *J. Appl. Phys.* **1995**, *77*, 2957−2973.
(28) Hoogsteen, W.; Postema, A.; Pennings, A.; Ten Brinke, G.; Zugenmaier, P. *Macromolecules* **1990**, *23*, 634−642.
(29) Puiggali, J.; Ikada, Y.; Tsuji, H.; Cartier, L.; Okihara, T.; Lotz, B. *Polymer* **2000**, *41*, 8921−8930.
(30) Cartier, L.; Okihara, T.; Ikada, Y.; Tsuji, H.; Puiggali, J.; Lotz, B. *Polymer* **2000**, *41*, 8909−8919.
(31) Kawai, T.; Rahman, N.; Matsuba, G.; Nishida, K.; Kanaya, T.; Nakano, M.; Okamoto, H.; Kawada, J.; Usuki, A.; Honma, N. *Macromolecules* **2007**, *40*, 9463−9469.
(32) Zhang, J.; Tashiro, K.; Tsuji, H.; Dombs, A. *Macromolecules* **2008**, *41*, 1352−1357.
(33) Chen, X. L.; Kalish, J.; Hsu, S. L. *J. Polym. Sci., Part B: Polym. Phys.* **2011**, *49*, 1446−1454.
(34) McGowan, J. C. *Polymer* **1969**, *10*, 841−848.
(35) Liu, J.; Jungnickel, B. J. *J. Polym. Sci., Part B: Polym. Phys.* **2007**, *45*, 1917−1931.
(36) Qiu, Z.; Ikehara, T.; Nishi, T. *Macromolecules* **2002**, *35*, 8251−8254.